nature structural & molecular biology

Initial activation of STIM1, the regulator of store-operated calcium entry

Yubin Zhou[1,3], Prasanna Srinivasan[1], Shiva Razavi[1], Sam Seymour[1], Paul Meraner[1], Aparna Gudlur[1], Peter B Stathopulos[2], Mitsuhiko Ikura[2], Anjana Rao[1] & Patrick G Hogan[1]

Physiological Ca^{2+} signaling in T lymphocytes and other cells depends on the STIM-ORAI pathway of store-operated Ca^{2+} entry. STIM1 and STIM2 are Ca^{2+} sensors in the endoplasmic reticulum (ER) membrane, with ER-luminal domains that monitor cellular Ca^{2+} stores and cytoplasmic domains that gate ORAI channels in the plasma membrane. The STIM ER-luminal domain dimerizes or oligomerizes upon dissociation of Ca^{2+}, but the mechanism transmitting activation to the STIM cytoplasmic domain was previously undefined. Using Tb^{3+}-acceptor energy transfer, we show that dimerization of STIM1 ER-luminal domains causes an extensive conformational change in mouse STIM1 cytoplasmic domains. The conformational change, triggered by apposition of the predicted coiled-coil 1 (CC1) regions, releases the ORAI-activating domains from their interaction with the CC1 regions and allows physical extension of the STIM1 cytoplasmic domain across the gap between ER and plasma membrane and communication with ORAI channels.

The Ca^{2+} release–activated Ca^{2+} (CRAC) current of T cells and mast cells[1–3] has been a classical example of store-operated Ca^{2+} entry (reviewed in ref. 4). The classical CRAC current is triggered by interaction of the ER Ca^{2+} sensor STIM1 with the plasma membrane Ca^{2+} channel ORAI1 (refs. 5–9). Inherited deficits in this pathway in humans and mice lead to immunodeficiency due to impaired function of T effector cells; autoimmune disease due to compromised function of T regulatory cells; and developmental disorders of muscle, skin, teeth and hair due to altered Ca^{2+} signaling in these tissues (reviewed in refs. 10,11). There is increasing evidence that the STIM1-ORAI1 pathway and CRAC current also contribute to Ca^{2+} signaling in other cells.

Store-operated Ca^{2+} entry is controlled by the ER-resident Ca^{2+} sensors STIM1 and STIM2 (refs. 5,6,12–16; reviewed in refs. 17–19). Physiological stimulation—through the T-cell receptor, the Fcε receptor of mast cells or various G protein–coupled receptors in other cells—initiates a sequence of ER Ca^{2+} depletion, dimerization or oligomerization of the STIM luminal domain and movement of STIM within the ER to sites where the ER is apposed to the plasma membrane (reviewed in refs. 17–19). The STIM cytoplasmic domain, through its SOAR(CAD) region, then recruits and directly activates the ORAI channel[20–25].

STIM1 at ER–plasma membrane junctions interacts with plasma membrane phosphoinositides, ORAI channels and other plasma membrane proteins[20–33]. Several of these interactions involve direct physical contact, in which STIM1 and its partner must bridge an ER–plasma membrane separation estimated at 10–25 nm (refs. 34–36). The interaction of a polybasic segment at the extreme C terminus of STIM1 with the plasma membrane lipid phosphatidylinositol 4,5-bisphosphate (PIP_2)[26–28,37] imposes a crucial geometric constraint. The PIP_2 head group is at the cytoplasmic face of the plasma membrane, and hence the cytoplasmic domain of STIM1 must itself bridge the distance from ER to plasma membrane.

To gain insight into the conformational changes in STIM1 that lead to store-operated Ca^{2+} entry, we mapped distances within STIM1 by Tb^{3+}-acceptor energy transfer[38,39]. The lanthanides Tb^{3+} and Eu^{3+} have favorable properties as donor fluorophores for distance measurements, as exemplified in studies of the protein conformations of myosin, the Shaker K^+ channel and RNA polymerase[40–43]. Moreover, the Tb^{3+} donor and its acceptor can be incorporated into STIM1 as small probes that are unlikely to cause appreciable changes in STIM1 conformations. Experiments described below indicate that the resting STIM1 cytoplasmic domain ($STIM1^{CT}$) in its preferred conformation does not span the >10 nm separating the ER and plasma membrane, thus implying that $STIM1^{CT}$ undergoes a substantial conformational change upon activation. Here we characterize this conformational change in biophysical and functional assays and delineate its mechanism.

RESULTS

'Activating' mutations increase $STIM1^{CT}$ binding to PIP_2

Initial targeting of STIM1 to the plasma membrane has been attributed to an interaction of the C-terminal polybasic segment of STIM1 with plasma membrane PIP_2 (refs. 26–28,37). We confirmed that $STIM1^{CT}$ binds PIP_2 and phosphatidylinositol 3,4,5-trisphosphate (PIP_3) in a commercially available array of seven phosphoinositides, phosphatidylinositol and certain other common membrane lipids (**Fig. 1a**) and binds PIP_2 in nanodiscs (**Fig. 1b** and **Supplementary Fig. 1a**),

[1]La Jolla Institute for Allergy & Immunology, La Jolla, California, USA. [2]Department of Medical Biophysics, University of Toronto, Toronto, Ontario, Canada. [3]Present address: Center for Translational Cancer Research, Institute of Biosciences & Technology, Texas A&M Health Science Center, Houston, Texas, USA. Correspondence should be addressed to P.G.H. (phogan@liai.org).

Received 11 February; accepted 21 May; published online 14 July 2013; doi:10.1038/nsmb.2625

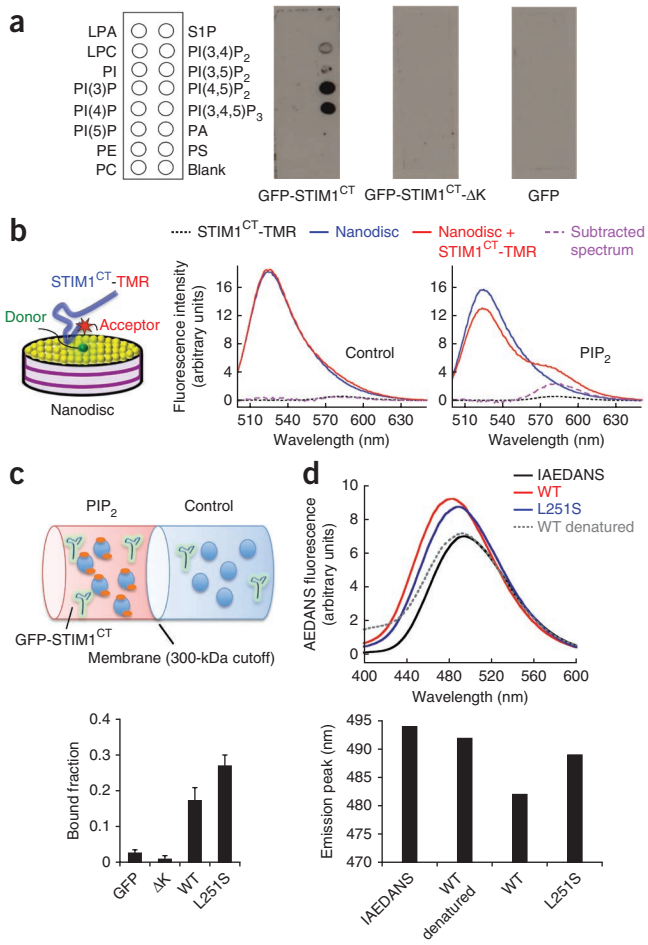

Figure 1 STIM1-PIP_2 interaction. (**a**) GFP-$STIM1^{CT}$ binding to PIP_2 and other lipids arrayed on a lipid strip. GFP-$STIM1^{CT}$ lacking the C-terminal polybasic segment (GFP-$STIM1^{CT}$-ΔK) and GFP alone are controls. LPA, lysophosphatidic acid; LPC, lysophosphatidylcholine; PI, phosphatidylinositol; PE, phosphatidylethanolamine; PC, phosphatidylcholine; S1P, sphingosine-1-phosphate; PA, phosphatidic acid; PS, phosphatidylserine. (**b**) GFP-$STIM1^{CT}$ binding to nanodiscs. Left, schematic of the experiment. A fluorescent phospholipid analog (1,2-dioleoyl-*sn*-glycero-3-phosphoethanolamine-N-(carboxyfluorescein)) serves as donor, and tetramethylrhodamine (TMR) attached to $STIM1^{CT}$ as acceptor. Center and right, binding measurements on control and PIP_2-containing nanodiscs, respectively. In the subtracted spectra, donor fluorescence was removed from the nanodisc + $STIM1^{CT}$ spectra by subtraction of an appropriately scaled nanodisc-alone spectrum. (**c**) GFP-$STIM1^{CT}$ binding to liposomes. Top, schematic of the equilibrium dialysis experiment. One chamber was loaded with PIP_2-containing liposomes, the other with control liposomes. The initial concentration of $STIM1^{CT}$ in the two chambers was identical. Bottom, excess GFP-$STIM1^{CT}$ recovered from the PIP_2 chamber after equilibration, as a fraction of total GFP-$STIM1^{CT}$ in both chambers. WT, wild type. Error bars, s.e.m. for three independent experiments. (**d**) Exposure of the $STIM1^{CT}$ C terminus, assessed with an environment-sensitive probe. Top, fluorescence spectra of IAEDANS and of AEDANS covalently attached to the indicated $STIM1^{CT}$ proteins at introduced residue Cys686. Bottom, wavelengths of peak fluorescence emission. The shift of the peak to a shorter wavelength in the wild-type protein is due to partial burial of the fluorophore. Representative of two experiments.

lipoprotein particles in which a belt of engineered apolipoprotein A1 scaffold protein surrounds a small circular lipid bilayer[44].

To dissect the targeting of activated STIM1, we examined the 'activated' STIM1 variant L251S, which has been shown to interact more effectively with ORAI1 than does wild-type STIM1 (ref. 45). We asked whether it also interacts more strongly with PIP_2. We quantified GFP-$STIM1^{CT}$ binding to liposomes, using an equilibrium dialysis assay, in which binding to PIP_2-containing liposomes is reflected in excess fluorescence in the PIP_2 chamber over that in the control chamber (**Fig. 1c** and **Supplementary Fig. 1b–d**). Binding is dependent on the STIM1 polybasic segment and is modestly increased by the L251S replacement (**Fig. 1c** and **Supplementary Fig. 1d**). The increased binding correlates with an increased exposure of the C-terminal polybasic segment of STIM1, as reported by the environment-sensitive fluorescent probe AEDANS introduced directly adjacent to the polybasic segment (**Fig. 1d**). Independent measurements of the exposure of the AEDANS fluorophore to collisional quenching of its fluorescence by acrylamide support this conclusion (**Supplementary Fig. 2a**,**b**).

Among several other STIM1 variants tested, only the activated variant ^{318}EEELE^{322}→AAALA (termed 4EA)[45,46] showed increased exposure of its C-terminal polybasic segment and an increased ability to interact with PIP_2 (**Supplementary Figs. 1d** and **2**). However, binding to PIP_2 remains weak, thus suggesting that an additional conformational change or other stabilizing factors contribute to stable STIM1 puncta formation in cells.

Activating mutations cause extension of $STIM1^{CT}$

Wild-type $STIM1^{CT}$ binds PIP_2 (**Fig. 1a–c**)[28] and ORAI1 (ref. 25) *in vitro*, and the soluble $STIM1^{CT}$ fragment expressed in cells binds and gates ORAI1 channels[20,25,47], results prompting the question of why STIM1 is inactive in resting cells. One hypothesis is that the cytoplasmic domain of STIM1 is retained near the ER until STIM1 is activated.

We used Tb^{3+}-acceptor energy transfer[38,39] to measure the distance between STIM1 residue 233—the site at which the cytoplasmic portion of STIM1 emerges from the ER membrane—and the STIM1 C-terminal polybasic tail that interacts with the plasma membrane (**Fig. 2a**). In the initial experiments, we compared unlabeled wild-type and L251S $STIM1^{CT}$ proteins. The wild-type protein is an elongated dimer that migrates ahead of compact globular proteins of comparable molecular weight in size-exclusion chromatography[25]. The L251S variant migrates slightly ahead of wild-type $STIM1^{CT}$ (**Fig. 2b** and **Supplementary Fig. 3**), reflecting a more extended conformation rather than increased oligomerization, on the basis of the finding that $STIM1_{234–491}$ with the L251S replacement is a dimer[45] and the direct distance measurements below. The CD spectrum of L251S variant $STIM1^{CT}$ reports no gross change in secondary structure (**Supplementary Fig. 3b**), but there is a subtle increase in thermal melting at temperatures below 40 °C that may reflect loss of an intramolecular interaction that stabilizes a portion of the α-helical secondary structure in the wild-type protein (**Fig. 2c**). On the basis of data presented below, it is likely that this is the intramolecular CC1-SOAR(CAD) interaction.

Tb^{3+} was excited through the lanthanide-binding-tag (LBT) tryptophan antenna by illumination at 280 nm, and energy transfer from Tb^{3+} to BODIPY FL was assessed in emission spectra gated at 200 μs to eliminate scattered light and fluorescence from direct excitation of acceptor. Protein labeled with Tb^{3+} donor alone displays the characteristic narrow Tb^{3+} emission peaks at 490 and 545 nm (**Fig. 2d**). Protein labeled with both donor and acceptor has, in addition, a broad BODIPY FL emission peak centered at 515 nm superimposed on the Tb^{3+} peaks (**Fig. 2d**). Control experiments established that the fluorescence peak at 515 nm is due to Tb^{3+}–BODIPY FL energy transfer within a $STIM1^{CT}$ dimer (**Supplementary Note**).

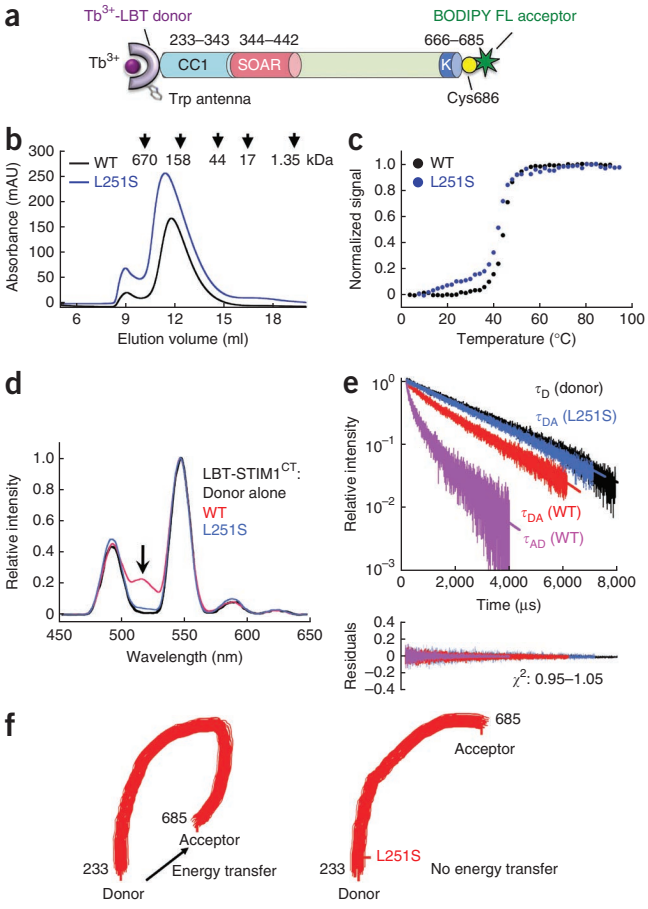

Figure 2 Distance measurements in STIM1 cytoplasmic domain. (**a**) Schematic of STIM1^{CT} donor-acceptor labeling. STIM1^{CT} C437S was engineered with an LBT[58] at its N terminus for labeling with donor Tb^{3+} and an added cysteine residue at its C terminus for labeling with acceptor fluorophore (**Supplementary Fig. 6**). SOAR, STIM1 Orai activating region; K, C-terminal polybasic tail. (**b**) Size-exclusion chromatography of wild-type and L251S variant STIM1^{CT} proteins. (**c**) Thermal melting monitored as change in CD at 222 nm, showing a difference in stability between wild-type STIM1^{CT} and the activated variant L251S at temperatures below 40 °C. (**d**) Gated luminescence spectra of labeled STIM1^{CT} proteins. Arrow indicates BODIPY FL acceptor emission from the labeled wild-type protein. (**e**) Luminescence decay of the indicated STIM1^{CT} proteins, followed at the donor wavelength in the absence and presence of acceptor (τ_D, τ_{DA}) and at the acceptor wavelength (τ_{AD}). Residuals indicate no systematic deviation of the data from the fitted curves. (**f**) Cartoon interpreting the results in **d** and **e**. The distance measured between residues 233 and 686 implies that the wild-type protein is folded back, whereas the activated L251S protein is extended.

Decay of Tb^{3+} luminescence in the presence of acceptor is a sensitive test of Tb^{3+}-acceptor energy transfer. LBT-STIM1^{CT} with Tb^{3+} donor alone exhibits a lifetime (τ) of ~2.32 ms (**Fig. 2e**), as expected for Tb^{3+} completely shielded from water by coordination to its LBT ligands[48–50]. In wild-type STIM1^{CT} labeled with BODIPY FL acceptor, Tb^{3+} emission exhibits a major quenched component having τ of ~1.21 ms and a second component having τ of ~0.28 ms (**Fig. 2e**, **Table 1** and **Supplementary Table 1**). A third component with τ of ~2.3 ms represents STIM1 not labeled with acceptor. The sensitized acceptor emission displays components with τ of ~0.98 ms and τ of ~0.21 ms (**Fig. 2e**, **Table 1** and **Supplementary Table 1**), in agreement with the quenched donor lifetimes. A straightforward interpretation is that there are two populations of wild-type STIM1^{CT} with different donor-acceptor distances of ~4.2 nm and ~3.0 nm (**Table 1** and **Supplementary Table 1**). An alternative dynamic interpretation (**Supplementary Note**) is that there is a single folded-back conformation with a donor-acceptor distance of ~3.1 nm and that the second time constant reflects conformational changes occurring during the excited-state lifetime of Tb^{3+} donor (**Table 2**). In either interpretation, extrapolation to STIM1 in cells suggests that wild-type STIM1^{CT} has a preferred conformation in which the polybasic segment at its C terminus is near the site of STIM1 anchoring in the ER and distant from the plasma membrane.

The gated spectrum of STIM1^{CT} variant L251S labeled with BODIPY FL shows very little sensitized acceptor signal (**Fig. 2d**) despite efficient labeling with acceptor (**Supplementary Fig. 3c**). Correspondingly, the donor lifetime in the presence of acceptor is only marginally less than the lifetime of donor alone (**Fig. 2e**, **Table 1** and **Supplementary Table 1**). To exclude bias introduced by the specific labeling strategy, we made independent measurements on LBT-STIM1^{CT} proteins labeled at the C terminus with a different acceptor fluorophore, BODIPY TMR (**Supplementary Fig. 4a–d**,

Table 1 Luminescence resonance energy transfer (LRET) distance estimates

			Donor emission at 490 nm or 545 nm			Acceptor emission at 515 nm or 570 nm		
Protein	Donor-acceptor pair	R_0 (Å)	τ_{DA} (μs (%))	E	R (Å)	τ_{AD} (μs (%))	E	R (Å)
Wild type	Tb^{3+}–BODIPY FL	44.0	277 (32)	0.88	31.5	206 (40)	0.91	29.8
			1,214 (41)	0.48	44.7	977 (60)	0.58	41.7
			2,317 (27)					
	Tb^{3+}–BODIPY TMR	54.3	189 (27)	0.92	36.3	189 (44)	0.92	36.3
			836 (32)	0.64	49.3	941 (56)	0.59	50.7
			2,359 (41)					
	Tb^{3+}-GFP	44.1	189 (29)	0.92	29.6	311 (15)	0.87	32.3
			1,036 (42)	0.55	42.6	1,081 (85)	0.53	43.1
			2,329 (29)					
L251S	Tb^{3+}–BODIPY FL	44.0	2,167 (100)	[0.066]	[68.4]	Negligible acceptor emission		
	Tb^{3+}–BODIPY TMR	54.3	2,208 (100)	[0.048]	[89.2]	Negligible acceptor emission		
	Tb^{3+}-GFP	44.1	2,164 (100)	[0.067]	[68.4]	Negligible acceptor emission		

Data have been fitted to a model in which energy transfer reports on two populations of STIM1^{CT} with distinct Tb^{3+}-acceptor distances. Tabulated values of τ_{DA} and τ_{AD} are averages from three experiments. Data from the individual experiments are listed in **Supplementary Table 1**. Amplitudes (%) of τ_{DA} and τ_{AD} have been corrected to zero time, and τ_{AD} has been corrected for energy-transfer rate as in ref. 59. All energy-transfer efficiency and distance calculations are based on τ_D of 2.32 ms. E is the efficiency of Tb^{3+}-acceptor energy transfer. R is the corresponding Tb^{3+}-acceptor distance. Bracketed values [] are outside the range for accurate estimation.

Table 2 LRET distance and conformational-change parameters

Protein	Donor-acceptor pair	R_0 (Å)	From donor emission					From acceptor emission				
			τ_1 (μs)	E	R (Å)	τ_{ex} (μs)	F	τ_1 (μs)	E	R (Å)	τ_{ex} (μs)	F
Wild type	Tb^{3+}–BODIPY FL	44.0	309	0.87	32.3	1,309	0.58	238	0.90	30.7	806	0.56
	Tb^{3+}–BODIPY TMR	54.3	215	0.91	37.2	716	0.63	213	0.91	37.1	820	0.59

The same data shown in **Table 1** have been fitted to a model in which $STIM1^{CT}$ has two states, a folded-back state in which energy transfer occurs and an extended state in which there is no energy transfer. The folded-back state extends with rate constant α, and the extended state folds back with rate constant β. Calculations are based on τ_D of 2.3 ms. τ_1 is the lifetime $(k_{transfer} + k_{Tb})^{-1}$ of excited Tb^{3+} in the folded-back state of $STIM1^{CT}$. E is the efficiency of Tb^{3+}-acceptor energy transfer in the folded-back state. R is the corresponding Tb^{3+}-acceptor distance. τ_{ex} is the characteristic time $(\alpha + \beta)^{-1}$ for exchange between the folded-back and extended states of $STIM1^{CT}$. F is the fraction of $STIM1^{CT}$ in the folded-back state.

Table 1 and **Supplementary Table 1**) and on $STIM1^{CT}$ proteins with a C-terminal Tb^{3+} donor and an N-terminal GFP acceptor (**Supplementary Fig. 4e–g**, **Table 1** and **Supplementary Table 1**). In each case, the wild-type donor-acceptor distance is 3–4 nm, and the L251S donor-acceptor distance falls beyond the range that can be estimated confidently with these donor-acceptor pairs, results indicating that the distance is increased in the L251S protein by at least 4–5 nm (**Fig. 2f**).

The other activating $STIM1^{CT}$ variant, 4EA, also has negligible energy transfer and negligible change in donor lifetime and thus has a large estimated donor-acceptor separation (**Supplementary Fig. 4h**,**i** and **Supplementary Table 1**). Three nonactivating variants of $STIM1^{CT}$ are similar to wild-type $STIM1^{CT}$ in their size-exclusion chromatography profiles (**Supplementary Fig. 3a**) and CD spectra (**Supplementary Fig. 3b**), and they do not differ appreciably from wild-type protein in the estimated distances between residue 233 and the polybasic tail (**Supplementary Table 1**).

CC1-CC1 association induces a conformational change

The CC1 region, $STIM1_{233–343}$, is positioned to take part both in bridging the distance between ER and plasma membrane and in propagating an activating conformational change in wild-type $STIM1^{CT}$. There has been a tacit belief that the basal state of CC1 is a coiled coil[51,52], though the primary STIM1 dimerization is through its SOAR(CAD) domain[23,53]. In fact, CC1 in isolation does not assemble as the predicted coiled coil. The molecular mass of the isolated recombinant CC1 fragment, estimated from size-exclusion chromatography coupled with multiangle light scattering (SEC-MALS), is 12.9 ± 1.1 kDa, comparable to the calculated monomer mass, 14.3 kDa (**Fig. 3a**). Notably, the CC1 regions are not closely associated in the context of the dimeric $STIM1^{CT}$ protein either, as established by a lack of intradimer energy transfer between donor and acceptor probes placed at the N termini of individual monomers within a $STIM1^{CT}$ dimer (**Fig. 3b–f**). For these experiments, we introduced a HAP2-peptide docking site for fluorescent α-bungarotoxin[54] at the

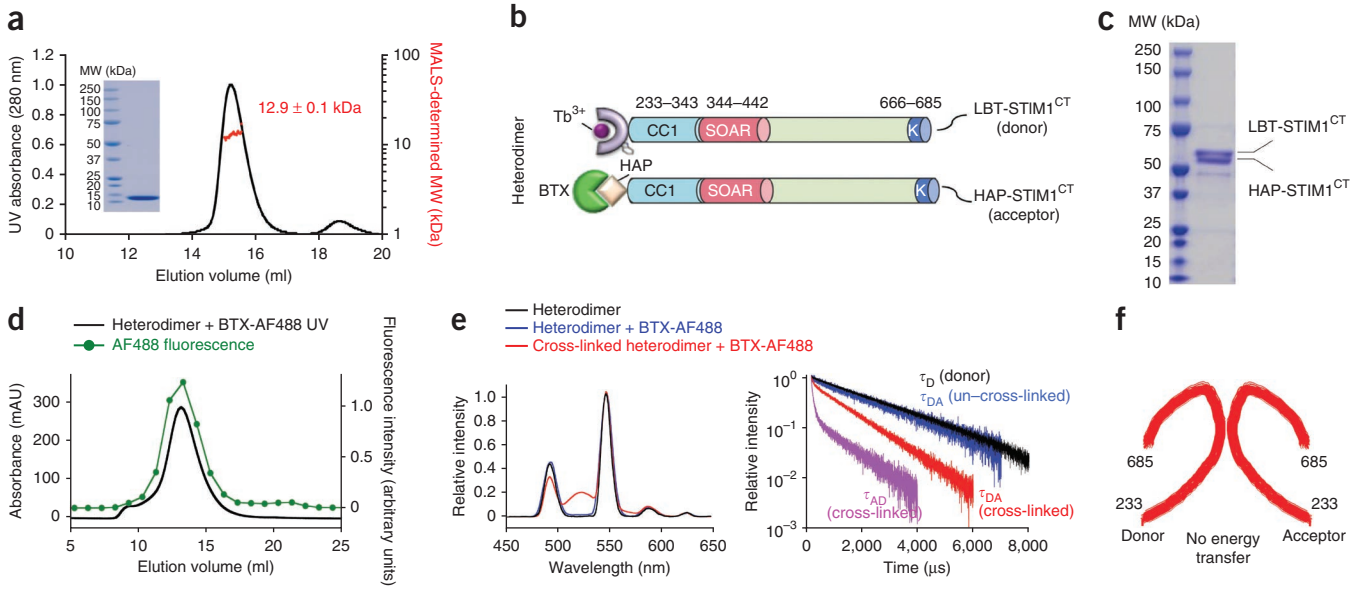

Figure 3 Lack of detectable CC1-CC1 association. (**a**) SEC-MALS determination of CC1 molecular weight (MW, right axis), plotted with the UV absorbance trace indicating the protein peak (left axis), showing that recombinant CC1 is monomeric. Inset, SDS-PAGE analysis of purified CC1. (**b**) Schematic of $STIM1^{CT}$ heterodimer in which one monomer was tagged at its N terminus with an LBT and the other monomer with a HAP peptide that binds the 8-kDa ligand α-bungarotoxin (BTX) with high affinity. Introduced cysteine residues used to cross-link the N termini are not shown. (**c**) SDS-PAGE analysis documenting that the heterodimer, as prepared, has roughly equal amounts of LBT-$STIM1^{CT}$ and HAP-$STIM1^{CT}$. (**d**) Size-exclusion chromatography showing formation of a stable complex of bound fluorescent α-bungarotoxin with $STIM1^{CT}$ protein. The UV absorbance signal from protein (black curve and left axis) and the fluorescence signal from Alexa Fluor 488 (AF488)–labeled α-bungarotoxin in fractions eluting from the column (green symbols and right axis) are plotted against elution volume. (**e**) Lack of CC1-CC1 association in dimeric $STIM1^{CT}$. Left, gated fluorescence spectra of the heterodimer with Tb^{3+} donor alone (black), un–cross-linked heterodimer with Tb^{3+} donor and fluorescent α-bungarotoxin acceptor (blue) and N-terminally cross-linked heterodimer with Tb^{3+} donor and fluorescent α-bungarotoxin acceptor (red). Right, corresponding luminescence decay curves. Tb^{3+} donor emission is shown except for τ_{AD}, for which acceptor emission is shown. (**f**) Cartoon illustrating the conclusion that the N termini of the individual $STIM1^{CT}$ monomers are not in proximity in the $STIM1^{CT}$ dimer.

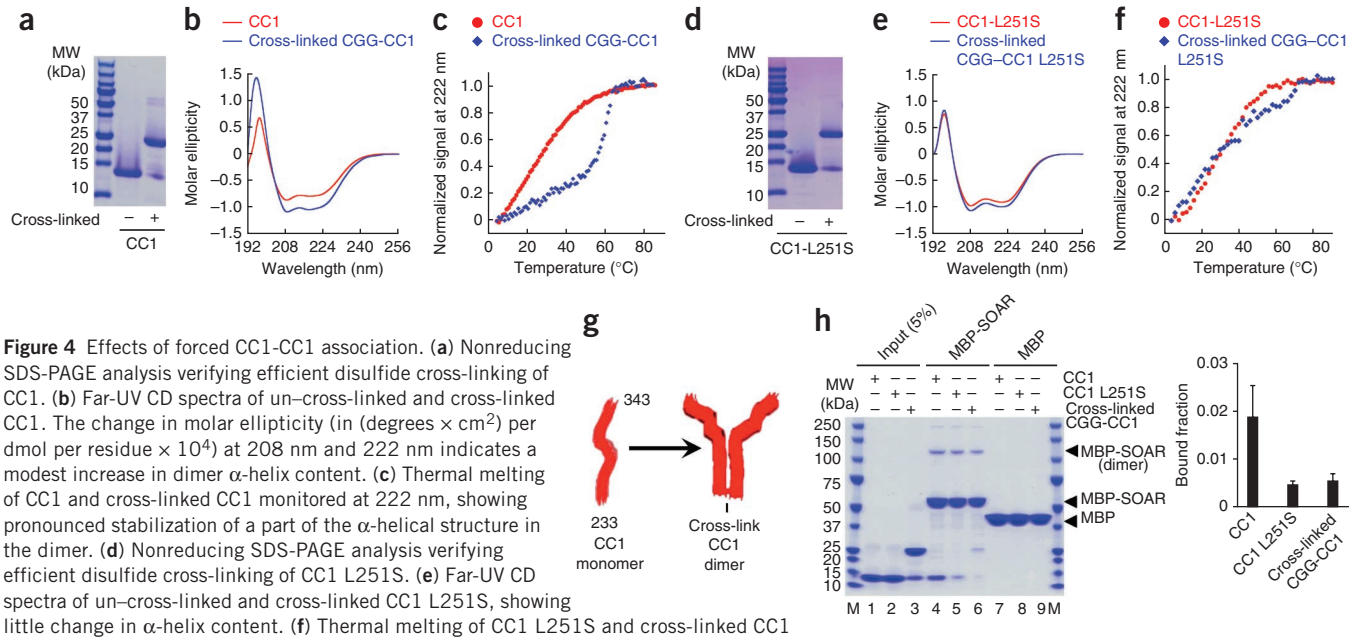

Figure 4 Effects of forced CC1-CC1 association. (**a**) Nonreducing SDS-PAGE analysis verifying efficient disulfide cross-linking of CC1. (**b**) Far-UV CD spectra of un–cross-linked and cross-linked CC1. The change in molar ellipticity (in (degrees × cm^2) per dmol per residue × 10^4) at 208 nm and 222 nm indicates a modest increase in dimer α-helix content. (**c**) Thermal melting of CC1 and cross-linked CC1 monitored at 222 nm, showing pronounced stabilization of a part of the α-helical structure in the dimer. (**d**) Nonreducing SDS-PAGE analysis verifying efficient disulfide cross-linking of CC1 L251S. (**e**) Far-UV CD spectra of un–cross-linked and cross-linked CC1 L251S, showing little change in α-helix content. (**f**) Thermal melting of CC1 L251S and cross-linked CC1 L251S monitored at 222 nm, showing failure of cross-linking to stabilize the secondary structure of CC1 L251S. (**g**) Cartoon of CC1 as the monomer or as the disulfide-linked dimer. (**h**) Binding of CC1, CC1 L251S and cross-linked dimeric CC1 to immobilized MBP-SOAR. Left, nonreducing SDS-PAGE analysis, representative of three experiments for CC1 and dimeric CC1 and two experiments for CC1 L251S. CGG denotes a Cys-Gly-Gly sequence engineered at the N terminus for cross-linking. M, marker. Right, quantification of the fraction of CC1 bound to MBP-SOAR. Mean ± s.e.m. of three independent experiments for CC1 and dimeric CC1; mean ± range of two independent experiments for CC1 L251S.

N terminus of $STIM1^{CT}$, coexpressed LBT-$STIM1^{CT}$ and HAP-$STIM1^{CT}$ and purified heterodimers bearing both a donor and an acceptor tag (**Supplementary Note**). Control experiments in which the N termini of the heterodimer were artificially brought together by a disulfide link verified that the assay detects CC1-CC1 proximity.

This finding led us to explore the hypothesis that bringing CC1 N termini together might trigger a conformational change. We first investigated the secondary structure of the recombinant CC1 monomer and of a CC1 dimer produced by engineering a disulfide bond between the N termini of CC1 monomers (**Fig. 4a** and **Supplementary Fig. 5a**). CD spectroscopy shows that the CC1 monomer has a modest content of α-helix at 4 °C, with a broad melting transition indicative of independent unfolding of parts of CC1 rather than concerted unfolding of a single compact domain (**Fig. 4b**,**c**). In contrast, the disulfide-linked dimer possesses increased α-helical secondary structure and, tellingly, exhibits a cooperative melting transition at ~60 °C, when the monomer is already fully denatured (**Fig. 4b**,**c**). Thus, physical apposition of the N termini of two CC1 monomers leads to increased CC1-CC1 interactions and a marked stabilization of a portion of CC1 secondary structure.

The effect of the L251S replacement casts light on the probable nature of the conformational change. The substitution does not, by itself, affect the thermal melting curve of the CC1 monomer (**Fig. 4d**–**f**). However, it prevents the stabilization of α-helical structure by forced dimerization. Given that L251 is in the core of the predicted coiled coil, and taking into account the fractional helix content stabilized, it is likely that the conformational change is the formation of a partial coiled coil (**Fig. 4g**).

CC1-CC1 association reduces interaction with SOAR(CAD)

A further key observation is that CC1 dimerization reduces the interaction between CC1 and SOAR(CAD), the minimal ORAI-activating domain within $STIM1^{CT}$. We purified monomeric CC1 and dimeric disulfide-linked CC1 and measured the interaction between these proteins and maltose-binding protein (MBP)-SOAR[53] immobilized on amylose resin. Comparison shows less binding of dimeric CC1 to SOAR(CAD) when equal amounts of CC1 protein are incubated (**Fig. 4h**, lanes 4 and 6). There is no binding to the MBP negative control (**Fig. 4h**). These findings are consistent with the hypothesis that bringing the N termini of CC1 into apposition within a $STIM1^{CT}$ dimer triggers a conformational change in CC1 and releases SOAR(CAD) from its interaction with CC1, thus resulting in extension of $STIM1^{CT}$.

The replacement L251S in CC1 likewise weakens the interaction between CC1 and MBP-SOAR (**Fig. 4h**). However, the activating mutation L251S and the activating conformational change triggered by CC1-CC1 interaction have a similar effect by different detailed mechanisms. On the basis of data shown above (**Fig. 4d**–**f**), the L251S replacement releases SOAR(CAD) without triggering the conformational change in CC1, thus suggesting that L251 either is part of the CC1-SOAR(CAD) interface in resting $STIM1^{CT}$ or participates in interactions that allosterically stabilize the interface. We propose that the key to STIM1 activation is the release of SOAR(CAD) and the polybasic tail from interactions that tether them near the ER. Active wild-type STIM1 achieves this by sequestering L251 in a CC1-CC1 coiled coil, thereby weakening the interaction with SOAR(CAD). The L251S replacement directly weakens the interaction with SOAR(CAD).

Intradimer CC1-CC1 association causes extension of $STIM1^{CT}$

Finally, we tested whether apposition of the N termini in $STIM1^{CT}$ can initiate a conformational change that propagates throughout $STIM1^{CT}$, using $STIM1^{CT}$ engineered with an LBT at the N terminus and a HAP2 docking site for fluorescent α-bungarotoxin at the C terminus of each monomer (**Fig. 5a**). An introduced cysteine at the extreme N terminus was either blocked by reaction with

iodoacetamide, to preclude oxidative cross-linking, or intentionally cross-linked with a bifunctional maleimide reagent (**Fig. 5b** and **Supplementary Fig. 5b**). LBT-STIM1^{CT}-HAP2 dimers with the N termini unconstrained recapitulate the energy transfer observed with other wild-type STIM1^{CT} proteins, thus indicating that the protein is in its folded-back conformation (**Fig. 5c**). In contrast, covalently cross-linked LBT-STIM1^{CT}-HAP2 dimers show no energy transfer in the gated spectra and no decrease in the Tb^{3+} luminescence lifetime, results reflecting an extended conformation (**Fig. 5c**). We conclude that apposition of the N termini of CC1 within a STIM1^{CT} dimer triggers a propagating conformational change that results in extension of STIM1^{CT} (**Fig. 5d**).

DISCUSSION

The initial step in STIM1 activation

Our findings have direct implications for the process of STIM1 activation and plasma membrane targeting in cells (**Fig. 6**). We have established here that CC1 regions do not associate detectably, either in isolation or when attached to SOAR(CAD). The isolated STIM1 ER-luminal domains also do not interact at Ca^{2+} concentrations typical of the ER in resting cells[13,16]. Nevertheless, the STIM1 cytoplasmic domain is clearly dimeric[25], with its primary dimerization through SOAR(CAD)[23]. Therefore we propose that the dimerized SOAR(CAD) regions are connected to the ER in resting cells by two physically independent CC1 tethers. Owing to the low density of native STIM1 in the ER, a decrease in luminal Ca^{2+} will elicit, preferentially, the association of the paired luminal domains within a STIM1 dimer. Association of the luminal domains will bring the initial portions of the CC1 regions into apposition, favor an otherwise weak CC1-CC1 interaction and trigger the physical extension of STIM1^{CT} and the enhanced exposure of the polybasic segment that interacts with PIP_2. A similar mechanism is likely to describe activation of STIM2.

The mechanism is roughly the converse of integrin inside-out signaling[55–57]. For integrin αβ dimers, protein-protein interactions at the cytoplasmic face of the plasma membrane, exemplified by talin binding to the integrin β subunit, allow the transmembrane segments of the α and β subunits to move apart, thus triggering an extension of the integrin extracellular domains and an increase in affinity for physiological integrin ligands. The detailed mechanisms of the STIM and integrin conformational changes are different, and for STIM it remains to be seen whether the transmembrane segments have a specific role other than to connect the luminal and cytoplasmic domains. However, a feature common to STIM1 and integrins is that the conformational change and clustering steps are distinct. In contrast, all previous models for STIM1 activation[15,19,26,45,46,52,53] have posited a single activation step tied to STIM oligomerization.

STIM-STIM FRET changes detected in cells

An increase in STIM-STIM FRET after store depletion was taken to indicate that oligomerization beyond the level of resting STIM1 is the first step in activation[26]. This view was supported by evidence that artificial oligomerization activates STIM[15] and by later STIM-STIM FRET experiments[47,52]. We have defined an activation mechanism initiated by the association of paired luminal domains within a pre-existing STIM dimer, an association that parallels the dimerization of recombinant STIM1 luminal domains observed in the absence of Ca^{2+} *in vitro*[13,16]. It is reasonable to ask whether there is a correlate in the cellular experiments. Is luminal dimer formation temporally separable in the cellular assays from higher-order oligomerization? Is it even detectable?

It can be argued that luminal-domain dimerization has gone undetected in cellular studies of full-length STIM1. A previous study showed, using a STIM protein (STIM1-ΔC) consisting of only the luminal domain and transmembrane segment, that the luminal domain alone cannot drive oligomerization to the extent observed with full-length STIM1 (ref. 52). The very small FRET signal from STIM1-ΔC at rest in those experiments could plausibly come from luminal-domain monomers, with the larger signal after store depletion reflecting the formation of luminal-domain dimers. In this view, because the FRET signal from CFP- and YFP-labeled full-length STIM at rest is already comparable to that from STIM1-ΔC luminal-domain dimers after store depletion, the initial step of luminal-domain association could be silent. Then the first step detected by FRET would be SOAR(CAD)-dependent oligomerization.

The high resting FRET signal in the case of full-length STIM1 deserves comment because it has two interpretations leading to

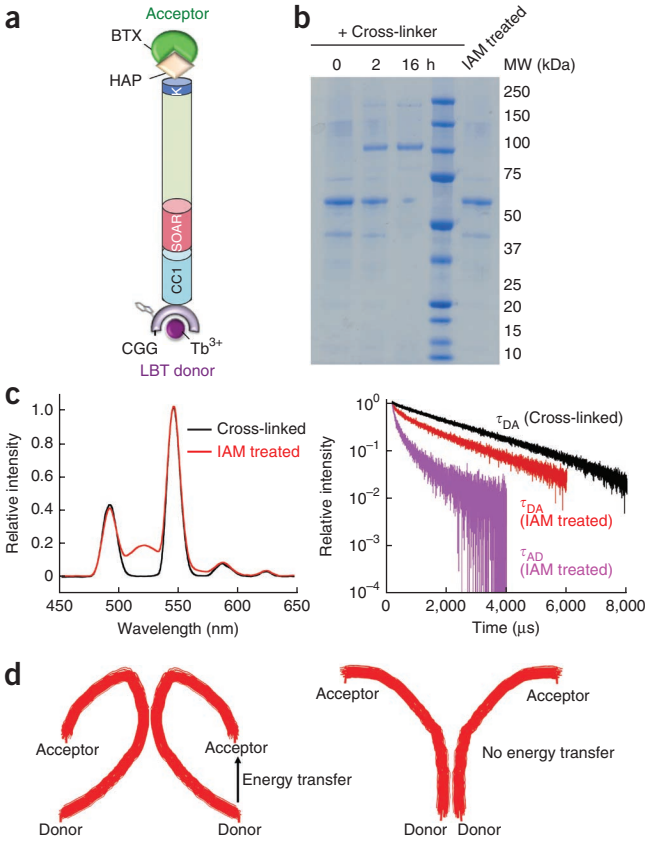

Figure 5 Intradimer CC1-CC1 association triggers extension of the STIM1 cytoplasmic domain. (**a**) Schematic illustrating the placement of labels, with an LBT binding Tb^{3+} at the N terminus of STIM1^{CT} and a HAP tag binding Alexa Fluor 488–labeled α-bungarotoxin at the C terminus. To allow cross-linking in this experiment, we introduced a cysteine residue at the extreme N terminus of STIM1^{CT}. (**b**) Reducing SDS-PAGE analysis documenting the effectiveness of cross-linking after a 16-h reaction. IAM, iodoacetamide. (**c**) CC1-CC1 cross-linking abolishes energy transfer between N-terminal donor and C-terminal acceptor. Left, gated fluorescence spectra of the iodoacetamide-blocked and cross-linked samples. Right, corresponding luminescence decay curves. Tb^{3+} donor emission was monitored except in the trace labeled τ_{AD} (magenta), for which acceptor emission was monitored. (**d**) Cartoon interpreting the results in **c**. CC1-CC1 cross-linking, like the L251S mutation, leads to an extended conformation of STIM1^{CT}.

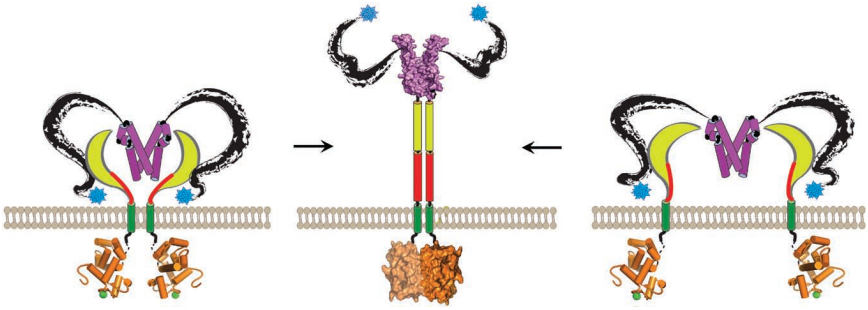

Figure 6 Model for STIM1 activation in cells. Left, inactive STIM1, showing individual CC1 regions (red and yellow) interacting with the SOAR(CAD) domains (magenta) (**Fig. 4h**), the relatively short distance between the N terminus of CC1 and the STIM1 C-terminal polybasic tail (blue) (**Fig. 2d**,**e**) and partial burial of the polybasic tail (**Fig. 1d**). STIM1 ER-luminal domain (brown) and SOAR(CAD) structures are as reported in the literature[16,53]. Detailed structural information for CC1 and for the region (black) C-terminal to SOAR(CAD) is not available. The model is not intended to specify the configuration of the polypeptide backbone that links CC1 to SOAR(CAD) or the surface(s) of SOAR(CAD) that are in contact with CC1. Right, an alternative possibility for inactive STIM1, with the N termini of its two CC1 segments separated (**Fig. 3e**). If L251 and SOAR(CAD) interact directly (**Fig. 4h**), the geometry of SOAR(CAD) in this case is likely to differ from that of the crystallized domain depicted. Center, active STIM1, with the initial portions of CC1 (red) coming together in a coiled coil (**Fig. 4a–f**), a loss of the CC1-SOAR(CAD) interaction (**Fig. 4h**) and an increased distance between the N terminus of CC1 and the polybasic tail (**Fig. 5c**). The structures of the luminal domain and of SOAR(CAD), rendered as solid dimers in active STIM1, have not been determined.

different conclusions about the configuration of unlabeled STIM1. In the first possibility, FRET between CFP- and YFP-labeled STIM proteins in resting cells accurately reflects the proximity of the transmembrane segments of the unlabeled STIM dimer in resting cells. This possibility must be taken seriously because the very pronounced conservation of the STIM1 transmembrane region across vertebrates could well indicate preservation of a sequence that allows a specific local rearrangement during activation. However, because we find that the two N termini of $STIM1^{CT}$ dimers in solution are well separated, this interpretation implies that there is an unidentified geometric constraint on full-length STIM1 in cells that does not apply to the isolated $STIM1^{CT}$ dimers. The second possibility is that the CFP and YFP labels in labeled STIM1 are appreciably closer together than are the transmembrane segments of the unlabeled STIM dimer. In that case, store depletion would induce both a substantial relative movement of the luminal domains and SOAR(CAD)-dependent oligomerization in unmodified wild-type STIM1. Both possibilities are represented in **Figure 6**.

CC1-CC1 interaction

A previous study also documented a CC1-CC1 interaction in an engineered STIM1 protein truncated after CC1 (STIM1-CC1)[52]. The protein-protein interaction was weak, in agreement with our observations on isolated CC1, stabilizing luminal-domain dimers for immunoprecipitation only in conditions of low Ca^{2+} and low-ionic-strength buffer. Yet, somewhat unexpectedly, FRET measurements indicated that the interaction resulted in dimerization of the luminal domains in resting cells[52]. Whereas the previous study[52] took this as evidence that CC1 supports the formation of inactive STIM1 oligomers in resting cells, we attribute the CC1-based dimerization in cells to the heightened CC1-CC1 interactions of overexpressed STIM1-CC1 confined to the ER membrane and the absence of competition from SOAR(CAD). Indeed, because loss of Ca^{2+} favors CC1-CC1 interaction, the converse is true as well, and the Ca^{2+} dependence of monomer-dimer equilibrium may shift so that the luminal domains of STIM1-CC1 are present as the Ca^{2+}-free dimer even before store depletion.

Earlier views of the activating conformational change

A pioneering study of activating mutations in the STIM1 cytoplasmic domain demonstrated that the 4EA variant of STIM1 is constitutively active[46]. It found further that artificial recruitment of a long CC1 fragment containing the EEELE sequence, $STIM1_{238–343}$, to the plasma membrane inhibited STIM-ORAI communication in a fraction of cells. On the basis of these data, the authors suggested that the acidic sequence interacts under resting conditions with a basic segment of $STIM1^{CT}$, thus masking the ORAI-interacting SOAR(CAD), and that STIM oligomerization unmasks SOAR(CAD). The specific interaction proposed is at variance with subsequently published structural evidence[53] and with the failure of the ^{382}KIKKK^{386}→QIQQQ mutant to cause extension of $STIM1^{CT}$ in the current study, but the notion that STIM oligomerization unmasks SOAR(CAD) has continued to resonate.

Another study characterized further mutations in CC1 and SOAR(CAD), assessed in the context of $STIM1_{233–474}$, termed ORAI1 activating small fragment or OASF[45]. Several of these mutations caused a reduction in the FRET signal from a CFP-OASF-YFP protein, thus indicating that the mutated OASF proteins assume a more extended conformation than does wild-type OASF. The conformational change correlated with activation of STIM1 in cases selected for examination because the mutant OASF proteins displayed increased binding to ORAI1 and because introduction of the substitutions into full-length STIM1 led to constitutive activation of ORAI1. On the basis of these findings, the authors proposed that physiological activation of STIM1 triggers oligomerization and conversion of the STIM1 cytoplasmic domain to an extended form[45], but they did not address the mechanism linking oligomerization and conformational change. The most potent single-residue changes identified in the FRET assay were substitutions at Leu251 or at Leu248, a neighboring residue predicted to be in the CC1 core, thus providing the first evidence that the initial region of CC1 is a determinant of the STIM1 resting conformation.

The recently published structure of a portion of *Caenorhabditis elegans* STIM-1 cytoplasmic domain (PDB 3TER) shows an α-helix spanning *C. elegans* STIM-1 residues 260–276 folded back against the SOAR domain[53]. This short segment, which corresponds to human STIM1 residues 318–334, was designated the inhibitory helix, though experimental support for the designation is limited to the activated phenotype of the human 4EA variant[46] and that of a variant produced by aggressive deletion of human STIM1 residues 310–337 (ref. 53). This interpretation of the structure led to a model in which store depletion causes the STIM1 luminal domain to dimerize or oligomerize, thus bringing about conformational changes in the inhibitory helices and release of SOAR(CAD). This proposal is more specific than the previous model[45], but, in focusing on the inhibitory helix, it is likely to reflect only one part of the CC1-SOAR interaction. First, *C. elegans* CC1 is considerably shorter than mammalian CC1, and the part of *C. elegans* CC1 resolved in the crystal structure comprises

only the 27 residues immediately N terminal to SOAR. Thus, a stretch of more than 80 residues of mammalian STIM1 CC1 is not represented, including an extensive region flanking Leu251. Second, the human ^{318}EEELE^{322} segment is present in the structure as *C. elegans* ^{260}HTEME^{264}, but, of these residues, only Glu264 is seen to make contact with SOAR(CAD). Most tellingly, the presence of the 'inhibitory helix' is not sufficient to maintain mammalian STIM1 in its inactive state because STIM1$_{315–462}$ is fully active[46], as is full-length STIM1 with the L251S substitution[45].

With our study, these proposals can be updated to incorporate a concrete mechanism in which luminal-domain association leads to CC1-CC1 association and the release of SOAR(CAD) and the STIM1 polybasic tail. Although the precise configuration of CC1 in the inactive STIM1 cytoplasmic domain remains to be defined, it seems likely that CC1 is folded against SOAR(CAD), with several regions including the segment around residues Leu248 and Leu251 contributing to maintenance of the inactive conformation. Our data suggest that CC1 redeploys upon activation as an extended α-helical structure with at least its N-terminal portion forming a coiled coil.

Conclusion

We have shown here that a key step in physiological activation of STIM1 is a conformational change that enables STIM1 to bridge the distance from ER to plasma membrane where it can engage PIP_2 and ORAI. The conformational change arises from the association of STIM1 ER-luminal domains and is independent of subsequent STIM oligomerization. Because this conformational rearrangement of the STIM1 dimer involves only two STIM1 Ca^{2+}-binding sites, the steep cooperativity of physiological STIM1 activation[14,15] must depend on further oligomerization following the initial activation step. It remains to be determined how higher-order STIM oligomerization is facilitated by the high local density of STIM1 at ER–plasma membrane junctions, by partner proteins and by binding to plasma membrane lipids or ORAI.

METHODS

Methods and any associated references are available in the online version of the paper.

Note: Supplementary information is available in the online version of the paper.

ACKNOWLEDGMENTS

This work was funded by US National Institutes of Health grants AI084167 and AI40127 (to A.R. and P.G.H.) and by grants from the Canadian Institutes of Health Research and the Heart and Stroke Foundation of Canada (to M.I.). Y.Z. has been supported by a postdoctoral fellowship from The Leukemia & Lymphoma Society (LLS) and by an LLS Special Fellow award, P.S. by a Human Frontier Science Program cross-disciplinary fellowship and A.G. by a Cancer Research Institute–Irvington Institute Fellowship. We thank Y. Shen (Nankai University, Tianjin, China) for the plasmid pMCSG9-SOAR and S. Sligar (University of Illinois Urbana-Champaign, Urbana, Illinois, USA) for the plasmid pMSP1D1.

AUTHOR CONTRIBUTIONS

Y.Z. and P.G.H. designed the study. Y.Z. designed engineered proteins, developed the assays and carried out the experiments with assistance from S.R. and S.S. P.S. made a detailed study of STIM1 binding to liposomes. P.M. prepared and characterized liposomes for the binding assays. A.G. contributed recombinant proteins and technical suggestions. P.B.S. and M.I. contributed the SEC-MALS characterization of recombinant CC1. Y.Z., A.R. and P.G.H. analyzed data, with input from the other authors. Y.Z. and P.G.H. wrote the manuscript.

COMPETING FINANCIAL INTERESTS

The authors declare competing financial interests: details are available in the online version of the paper.

1. Hoth, M. & Penner, R. Depletion of intracellular calcium stores activates a calcium current in mast cells. *Nature* **355**, 353–356 (1992).
2. Hoth, M. & Penner, R. Calcium release-activated calcium current in rat mast cells. *J. Physiol.* (*Lond.*) **465**, 359–386 (1993).
3. Zweifach, A. & Lewis, R.S. Mitogen-regulated Ca^{2+} current of T lymphocytes is activated by depletion of intracellular Ca^{2+} stores. *Proc. Natl. Acad. Sci. USA* **90**, 6295–6299 (1993).
4. Parekh, A.B. & Putney, J.W. Jr. Store-operated calcium channels. *Physiol. Rev.* **85**, 757–810 (2005).
5. Roos, J. *et al.* STIM1, an essential and conserved component of store-operated Ca^{2+} channel function. *J. Cell Biol.* **169**, 435–445 (2005).
6. Liou, J. *et al.* STIM is a Ca^{2+} sensor essential for Ca^{2+} -store-depletion-triggered Ca^{2+} influx. *Curr. Biol.* **15**, 1235–1241 (2005).
7. Feske, S. *et al.* A mutation in Orai1 causes immune deficiency by abrogating CRAC channel function. *Nature* **441**, 179–185 (2006).
8. Vig, M. *et al.* CRACM1 is a plasma membrane protein essential for store-operated Ca^{2+} entry. *Science* **312**, 1220–1223 (2006).
9. Zhang, S.L. *et al.* Genome-wide RNAi screen of Ca^{2+} influx identifies genes that regulate Ca^{2+} release-activated Ca^{2+} channel activity. *Proc. Natl. Acad. Sci. USA* **103**, 9357–9362 (2006).
10. Feske, S. ORAI1 and STIM1 deficiency in human and mice: roles of store-operated Ca^{2+} entry in the immune system and beyond. *Immunol. Rev.* **231**, 189–209 (2009).
11. Feske, S. Immunodeficiency due to defects in store-operated calcium entry. *Ann. NY Acad. Sci.* **1238**, 74–90 (2011).
12. Zhang, S.L. *et al.* STIM1 is a Ca^{2+} sensor that activates CRAC channels and migrates from the Ca^{2+} store to the plasma membrane. *Nature* **437**, 902–905 (2005).
13. Stathopulos, P.B., Li, G.Y., Plevin, M.J., Ames, J.B. & Ikura, M. Stored Ca^{2+} depletion-induced oligomerization of stromal interaction molecule 1 (STIM1) via the EF-SAM region: an initiation mechanism for capacitative Ca^{2+} entry. *J. Biol. Chem.* **281**, 35855–35862 (2006).
14. Brandman, O., Liou, J., Park, W.S. & Meyer, T. STIM2 is a feedback regulator that stabilizes basal cytosolic and endoplasmic reticulum Ca^{2+} levels. *Cell* **131**, 1327–1339 (2007).
15. Luik, R.M., Wang, B., Prakriya, M., Wu, M.M. & Lewis, R.S. Oligomerization of STIM1 couples ER calcium depletion to CRAC channel activation. *Nature* **454**, 538–542 (2008).
16. Stathopulos, P.B., Zheng, L., Li, G.Y., Plevin, M.J. & Ikura, M. Structural and mechanistic insights into STIM1-mediated initiation of store-operated calcium entry. *Cell* **135**, 110–122 (2008).
17. Cahalan, M.D. STIMulating store-operated Ca^{2+} entry. *Nat. Cell Biol.* **11**, 669–677 (2009).
18. Hogan, P.G., Lewis, R.S. & Rao, A. Molecular basis of calcium signaling in lymphocytes: STIM and ORAI. *Annu. Rev. Immunol.* **28**, 491–533 (2010).
19. Soboloff, J., Rothberg, B.S., Madesh, M. & Gill, D.L. STIM proteins: dynamic calcium signal transducers. *Nat. Rev. Mol. Cell Biol.* **13**, 549–565 (2012).
20. Huang, G.N. *et al.* STIM1 carboxyl-terminus activates native SOC, I_{crac} and TRPC1 channels. *Nat. Cell Biol.* **8**, 1003–1010 (2006).
21. Yuan, J.P. *et al.* SOAR and the polybasic STIM1 domains gate and regulate Orai channels. *Nat. Cell Biol.* **11**, 337–343 (2009).
22. Park, C.Y. *et al.* STIM1 clusters and activates CRAC channels via direct binding of a cytosolic domain to Orai1. *Cell* **136**, 876–890 (2009).
23. Muik, M. *et al.* A cytosolic homomerization and a modulatory domain within STIM1 C terminus determine coupling to ORAI1 channels. *J. Biol. Chem.* **284**, 8421–8426 (2009).
24. Kawasaki, T., Lange, I. & Feske, S. A minimal regulatory domain in the C terminus of STIM1 binds to and activates ORAI1 CRAC channels. *Biochem. Biophys. Res. Commun.* **385**, 49–54 (2009).
25. Zhou, Y. *et al.* STIM1 gates the store-operated calcium channel ORAI1 *in vitro*. *Nat. Struct. Mol. Biol.* **17**, 112–116 (2010).
26. Liou, J., Fivaz, M., Inoue, T. & Meyer, T. Live-cell imaging reveals sequential oligomerization and local plasma membrane targeting of stromal interaction molecule 1 after Ca^{2+} store depletion. *Proc. Natl. Acad. Sci. USA* **104**, 9301–9306 (2007).
27. Walsh, C.M. *et al.* Role of phosphoinositides in STIM1 dynamics and store-operated calcium entry. *Biochem. J.* **425**, 159–168 (2009).
28. Ercan, E. *et al.* A conserved, lipid-mediated sorting mechanism of yeast Ist2 and mammalian STIM proteins to the peripheral ER. *Traffic* **10**, 1802–1818 (2009).
29. Frischauf, I. *et al.* Molecular determinants of the coupling between STIM1 and Orai channels: differential activation of Orai1–3 channels by a STIM1 coiled-coil mutant. *J. Biol. Chem.* **284**, 21696–21706 (2009).
30. Zeng, W. *et al.* STIM1 gates TRPC channels, but not Orai1, by electrostatic interaction. *Mol. Cell* **32**, 439–448 (2008).
31. Lefkimmiatis, K. *et al.* Store-operated cyclic AMP signalling mediated by STIM1. *Nat. Cell Biol.* **11**, 433–442 (2009).
32. Park, C.Y., Shcheglovitov, A. & Dolmetsch, R. The CRAC channel activator STIM1 binds and inhibits L-type voltage-gated calcium channels. *Science* **330**, 101–105 (2010).

33. Wang, Y. *et al.* The calcium store sensor, STIM1, reciprocally controls Orai and $Ca_V1.2$ channels. *Science* **330**, 105–109 (2010).
34. Wu, M.M., Buchanan, J., Luik, R.M. & Lewis, R.S. Ca^{2+} store depletion causes STIM1 to accumulate in ER regions closely associated with the plasma membrane. *J. Cell Biol.* **174**, 803–813 (2006).
35. Várnai, P., Tóth, B., Tóth, D.J., Hunyady, L. & Balla, T. Visualization and manipulation of plasma membrane-reticulum contact sites indicates the presence of additional molecular components within the STIM1-Orai1 complex. *J. Biol. Chem.* **282**, 29678–29690 (2007).
36. Orci, L. *et al.* STIM1-induced precortical and cortical subdomains of the endoplasmic reticulum. *Proc. Natl. Acad. Sci. USA* **106**, 19358–19362 (2009).
37. Carrasco, S. & Meyer, T. STIM proteins and the endoplasmic reticulum-plasma membrane junctions. *Annu. Rev. Biochem.* **80**, 973–1000 (2011).
38. Selvin, P.R. & Hearst, J.E. Luminescence energy transfer using a terbium chelate: improvements on fluorescence energy transfer. *Proc. Natl. Acad. Sci. USA* **91**, 10024–10028 (1994).
39. Selvin, P.R. Principles and biophysical applications of lanthanide-based probes. *Annu. Rev. Biophys. Biomol. Struct.* **31**, 275–302 (2002).
40. Xiao, M. *et al.* An actin-dependent conformational change in myosin. *Nat. Struct. Biol.* **10**, 402–408 (2003).
41. Cha, A., Snyder, G.E., Selvin, P.R. & Bezanilla, F. Atomic scale movement of the voltage-sensing region in a potassium channel measured via spectroscopy. *Nature* **402**, 809–813 (1999).
42. Posson, D.J., Ge, P., Miller, C., Bezanilla, F. & Selvin, P.R. Small vertical movement of a K^+ channel voltage sensor measured with luminescence energy transfer. *Nature* **436**, 848–851 (2005).
43. Callaci, S., Heyduk, E. & Heyduk, T. Core RNA polymerase from *E. coli* induces a major change in the domain arrangement of the σ^{70} subunit. *Mol. Cell* **3**, 229–238 (1999).
44. Nath, A., Atkins, W.M. & Sligar, S.G. Applications of phospholipid bilayer nanodiscs in the study of membranes and membrane proteins. *Biochemistry* **46**, 2059–2069 (2007).
45. Muik, M. *et al.* STIM1 couples to ORAI1 via an intramolecular transition into an extended conformation. *EMBO J.* **30**, 1678–1689 (2011).
46. Korzeniowski, M.K., Manjarrés, I.M., Várnai, P. & Balla, T. Activation of STIM1-Orai1 involves an intramolecular switching mechanism. *Sci. Signal.* **3**, ra82 (2010).
47. Muik, M. *et al.* Dynamic coupling of the putative coiled-coil domain of ORAI1 with STIM1 mediates ORAI1 channel activation. *J. Biol. Chem.* **283**, 8014–8022 (2008).
48. Horrocks, W.D. Jr. & Sudnick, D.R. Lanthanide ion probes of structure in biology. Laser-induced luminescence decay constants provide a direct measure of the number of metal-coordinated water molecules. *J. Am. Chem. Soc.* **101**, 334–340 (1979).
49. Beeby, A. *et al.* Non-radiative deactivation of the excited states of europium, terbium and ytterbium complexes by proximate energy-matched OH, NH and CH oscillators: an improved luminescence method for establishing solution hydration states. *J. Chem. Soc. Perkin Trans.* **2**, 493–503 (1999).
50. Martin, L. *Development of lanthanide-binding tags (LBTs) as powerful and versatile peptides for use in studies of proteins and protein interactions*. PhD thesis, Massachusetts Inst. of Technology (2008).
51. Williams, R.T. *et al.* Identification and characterization of the STIM (stromal interaction molecule) gene family: coding for a novel class of transmembrane proteins. *Biochem. J.* **357**, 673–685 (2001).
52. Covington, E.D., Wu, M.M. & Lewis, R.S. Essential role for the CRAC activation domain in store-dependent oligomerization of STIM1. *Mol. Biol. Cell* **21**, 1897–1907 (2010).
53. Yang, X., Jin, H., Cai, X., Li, S. & Shen, Y. Structural and mechanistic insights into the activation of Stromal interaction molecule 1 (STIM1). *Proc. Natl. Acad. Sci. USA* **109**, 5657–5662 (2012).
54. Katchalski-Katzir, E. *et al.* Design and synthesis of peptides that bind α-bungarotoxin with high affinity and mimic the three-dimensional structure of the binding-site of acetylcholine receptor. *Biophys. Chem.* **100**, 293–305 (2003).
55. Lau, T.L., Kim, C., Ginsberg, M.H. & Ulmer, T.S. The structure of the integrin αIIbβ3 transmembrane complex explains integrin transmembrane signalling. *EMBO J.* **28**, 1351–1361 (2009).
56. Anthis, N.J. *et al.* The structure of an integrin talin complex reveals the basis of inside-out signal transduction. *EMBO J.* **28**, 3623–3632 (2009).
57. Kim, C., Ye, F. & Ginsberg, M.H. Regulation of integrin activation. *Annu. Rev. Cell Dev. Biol.* **27**, 321–345 (2011).
58. Sculimbrene, B.R. & Imperiali, B. Lanthanide-binding tags as luminescent probes for studying protein interactions. *J. Am. Chem. Soc.* **128**, 7346–7352 (2006).
59. Heyduk, T. & Heyduk, E. Luminescence energy transfer with lanthanide chelates: interpretation of sensitized acceptor decay amplitudes. *Anal. Biochem.* **289**, 60–67 (2001).

ONLINE METHODS

Engineered proteins. STIM1^{CT}, its fragments CC1, SOAR(CAD) (as the MBP-SOAR fusion protein[53]) and STIM1^{CT}-ΔK, STIM1 variants and GFP-STIM1^{CT} variants were expressed in *E. coli* and purified with standard techniques. Short LBT[58] or HAP-tag[54] sequences were inserted into the proteins as indicated, for labeling, respectively, with Tb^{3+} as donor fluorophore or with α-bungarotoxin carrying an acceptor fluorophore. Cysteine residues for covalent labeling or for cross-linking were engineered into cysteine-less STIM1^{CT} C437S or into the CC1 fragment, and fluorescent labels were incorporated as indicated. The recombinant proteins were characterized by FPLC, CD spectroscopy, SEC-MALS, and reducing and nonreducing SDS-PAGE.

Fluorescence spectroscopy. Fluorescence spectra and emission-decay measurements were acquired with a QM40 spectrofluorometer (Photon Technology International). Tb^{3+} luminescence and Tb^{3+}-sensitized acceptor emission were excited at 280 nm and AEDANS fluorescence at 335 nm. Gated fluorescence spectra and emission-decay measurements used a pulsed xenon excitation source. The decay of Tb^{3+} emission was monitored at 490 nm or at 545 nm, and the decay of acceptor emission at 515 nm or at 570 nm, as appropriate. Data collection was from 200 μs to 10 ms, and 3,000 shots were averaged. Protein concentration in the Tb^{3+}-acceptor energy-transfer experiments was below 300 nM, and the measurements were made at 4 °C in buffer containing 80% glycerol to avoid diffusion-enhanced energy transfer to bystander molecules (**Supplementary Fig. 6d**,**e**).

Distance estimates. Emission-decay curves were fitted to a sum of one, two or three exponentials with Felix GX software supplied with the spectrofluorometer. Energy-transfer efficiency E and donor-acceptor distance R were calculated with the equations for Förster energy transfer[39]. Because each STIM1^{CT} protein for which energy transfer was observed yielded two distinct decay constants corresponding to Tb^{3+}-acceptor energy transfer, this conventional treatment resulted in two distance estimates for each case and an estimate of the relative occupancies of the corresponding conformations. Although there is no compelling evidence that a fraction of wild-type STIM1^{CT} can assume an extended conformation in which there is no energy transfer, the negligible energy transfer in the L251S variant establishes the existence of such an extended conformation in activated forms of STIM1. Hence the data were also fitted to an alternative model with a single conformation exhibiting energy transfer, an extended conformation in which there is no energy transfer and exchange between the two conformations during the lifetime of excited Tb^{3+}. Details are provided in **Supplementary Note**. This fitting procedure results in estimates of a single donor-acceptor distance, a rate of exchange between the conformations and the relative occupancies of the two conformations in equilibrium.

STIM1-PIP_2 binding. For the nanodisc binding assay, membrane scaffold protein 1D1 (MSP1D1) was purified and assembled into nanodiscs with 1,2-dimyristoyl-*sn*-glycero-3-phosphocholine (DMPC)[60]. The fluorescent lipid 1,2-dioleoyl-*sn*-glycero-3-phosphoethanolamine-N-(carboxyfluorescein) (PE-CF) was incorporated into the nanodiscs as a donor fluorophore. In control nanodiscs, the DMPC/PE-CF ratio was 79:1. In nanodiscs containing PIP_2, the DMPC/PE-CF/ PIP_2 ratio was 79:1:2. STIM1^{CT}-TMR was titrated into a nanodisc sample at concentrations up to 2 μM, and STIM1-nanodisc binding was monitored by measurements of PE-CF–sensitized TMR fluorescence emission, with excitation at 450 nm to minimize direct excitation of acceptor.

Binding of GFP-STIM1^{CT} to PIP_2-containing liposomes was assessed quantitatively in a two-chamber microdialysis assay. Control liposomes consisted of 1-palmitoyl-2-oleoyl-*sn*-glycero-3-phosphocholine (POPC), 1-palmitoyl-2-oleoyl-*sn*-glycero-3-phospho-L-serine (POPS), and 1-palmitoyl-2-oleoyl-*sn*-glycero-3-phosphoethanolamine (POPE) in a 4:1:2 molar ratio. PIP_2 liposomes contained additionally 2 mol% PIP_2 unless a different PIP_2 content was specified. For the assay, a microdialysis cell of 200-μL total capacity was divided into two equal chambers by a cellulose acetate membrane with a nominal molecular-weight cutoff of 300 kDa, permeable to GFP-STIM1^{CT} but not to the substantially larger liposomes. The cell was loaded initially with PIP_2 liposomes and GFP-STIM1^{CT} or the indicated GFP-STIM1^{CT} variant (10 nM) in one dialysis chamber, and with control liposomes and the same protein at the same concentration in the other chamber. After equilibration, GFP fluorescence was determined in samples recovered from each chamber and corrected for the scattering signal due to the liposomes, and the fraction of GFP-STIM1^{CT} bound was calculated as $(F_{PIP2} - F_{control}) / (F_{control} + F_{PIP2})$, where F_{PIP2} is the fluorescence intensity in the chamber with PIP_2 liposomes and $F_{control}$ is the fluorescence intensity in the control chamber.

CC1-SOAR(CAD) interaction. MBP or MBP-SOAR was immobilized on amylose resin, incubated for 4 h at 4 °C with 400 μg of the recombinant CC1 protein indicated and washed extensively. Bound protein was analyzed by nonreducing SDS-PAGE. Protein bands stained with Coomassie Brilliant Blue R-250 were quantified with ImageJ (http://rsbweb.nih.gov/ij/).

Data analysis and statistics. Error bars indicate mean ± s.e.m., except in the case of CC1 L251S (**Fig. 4h**), where they indicate the range. Because fitted lifetimes need not be distributed according to a Gaussian function, mean values are reported in **Table 1** without an attempt to estimate statistical variability, and the actual fitted values from all experiments are reported in **Supplementary Table 1**.

60. Ritchie, T.K. *et al.* Chapter 11: reconstitution of membrane proteins in phospholipid bilayer nanodiscs. *Methods Enzymol.* **464**, 211–231 (2009).

doi:10.1038/nsmb|2625